Co Huynh
Liping Zheng
Dipjyoti Acharya

Calnetix, Inc.,
Cerritos, CA 90703

Losses in High Speed Permanent Magnet Machines Used in Microturbine Applications

High speed permanent magnet (PM) machines are used in microturbine applications due to their compactness, robust construction, and high efficiency characteristics. These machines are integrated with the turbines and rotate at the same speeds. This paper discusses in detail the losses in high speed PM machines. A typical PM machine designed for microturbine application is presented with its detailed loss calculations. Various loss verification methods are also discussed. [DOI: 10.1115/1.2982151]

1 Introduction

Microturbines are small combustion turbines with typical outputs in the range of 20–500 kW. A typical system rotates over 40,000 rpm. One of the key enabling technologies for microturbines is the integral high speed electrical machines operating at the same speeds as the turbines, eliminating mechanical gearboxes. The result is a very compact high efficiency system that allows for ease of onsite installation. High speed permanent magnet (PM) machines are typically used in microturbine application due to their high power density and high efficiency characteristics. A good understanding of high speed PM machine characteristics, especially its losses, is critical to predict system performance and to ensure a reliable operation.

Losses in PM machines can be divided into three categories: (a) stator loss, (b) rotor eddy current loss, and (c) windage loss. The stator loss consists of copper loss and iron loss. The copper loss includes conventional I^2R loss and stray load loss due to skin effect and proximity effect. This can be calculated based on finite element analysis (FEA) or using analytical methods. The stator iron loss is divided into hysteresis loss, classical eddy current loss, and excess eddy current loss. Empirical equations or time-step transient FEA with motion can be used to calculate iron loss. The rotor loss generated by induced eddy currents in the steel shaft and permanent magnets is not significant compared with a machine's total loss. However, removing the heat from the rotor to ensure reasonable operating temperatures of its components is more difficult than removing the heat from the stator. Thus, an accurate prediction of rotor loss becomes important especially at high speed. The major causes of the rotor loss are (a) space harmonics due to the existence of stator slot opening and winding distribution and (b) time harmonics of the phase currents due to pulse width modulation (PWM). The rotor loss can be analyzed using analytical methods. However, simulations using FEA based on actual measured current waveforms or estimated current with total harmonics distortion (THD) provide a more accurate assessment. The windage loss as a result of the shearing action of the media that exists between the rotor and stator may also be significant at high speed, especially with small air gap and high cooling flow pressure in the air gap between the rotor and stator.

A spin-down test can be used to verify no-load loss, especially when the rotor's inertia is large. Testing of a back-to-back configuration can verify a machine's efficiencies and total losses at various loaded conditions. The thermal analysis model result compared with measured temperature mapping can also be used to verify machine losses.

2 Permanent Magnet Alternator Losses

The losses in PM alternators are grouped into (a) stator loss, (b) rotor eddy current loss, and (c) windage loss.

2.1 Stator Loss. The stator loss consists of copper loss and iron loss. Copper loss is the loss due to the current going through the armature windings. The copper loss consists of I^2R loss and stray load loss. The I^2R loss is given by

$$P_{\text{cu}} = m_1 I^2 R \tag{1}$$

where m_1 is the number of phases, I is the armature current, and R is the dc armature resistance. The I^2R loss can be significant when large current flows through the conductor with large Ohmic resistance.

The stray loss comes from (a) the skin effect resulting from the same source conductors and (b) the proximity effect resulting from the field induced from adjacent conductors sharing the same slot. The skin effect is caused by electromagnetic induction in the conducting material, which opposes the currents set up by the wave E-field. The skin depth is the distance in which an electromagnetic wave entering a conducting surface is damped and reduces in amplitude by a factor of $1/e$, where e is equal to 2.71828…. The skin depth (δ) is given by

$$\delta = \sqrt{\frac{2}{\omega \mu_0 \sigma}} \tag{2}$$

where ω is the angular frequency of the current and σ is the electrical conductivity of the conducting material.

In designing the stator winding, wire strand size is selected such that skin depth is much larger than the wire radius to minimize loss due to skin effect.

Stator windings are contained inside slots. Loss due to proximity effects of conductors located in the slots of electric machines can be estimated based on the following equation [1]:

$$P_{\text{stray}} = P_{\text{cu}}(k_d - 1) \tag{3}$$

where

$$k_d = \varphi(\xi) + \left[\frac{m^2 - 1}{3} - \left(\frac{m}{2}\sin\left(\frac{\gamma}{2}\right)\right)^2\right]\psi(\xi) \tag{4}$$

$$\varphi(\xi) = \xi\frac{\sinh(2\xi) + \sin(2\xi)}{\cosh(2\xi) - \cos(2\xi)} \tag{5}$$

Contributed by the International Gas Turbine Institute of ASME for publication in the JOURNAL OF ENGINEERING FOR GAS TURBINES AND POWER. Manuscript received April 1, 2008; final manuscript received May 9, 2008; published online December 23, 2008. Review conducted by Dilip R. Ballal. Paper presented at the ASME Turbo Expo 2008: Land, Sea and Air (GT2008), Berlin, Germany, June 9–13, 2008.

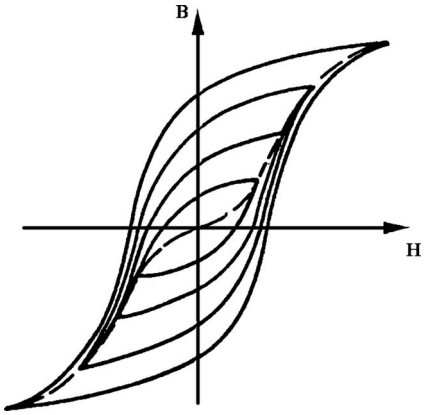

Fig. 1 Family of hysteresis loops

$$\psi(\xi) = 2(\xi)\frac{\sinh(\xi) - \sin(\xi)}{\cosh(\xi) + \cos(\xi)} \tag{6}$$

and ξ is the relative height of a conductor (the ratio of its height to the effective skin depth δ considering insulation). γ is the phase angle between the upper layer and lower layer currents for a two-layer case, m is the total number of identical conductors in layers, and kd is the average resistance coefficient, which is the ratio of effective ac resistance versus dc resistance.

The copper loss is temperature dependent, so the copper loss is calculated at the expected copper temperature. The copper I^2R loss increases when copper temperature increases due to increased winding resistance, while the copper stray load loss reduces with increased temperature. In addition to the analytical method described above, loss due to proximity and skin effects can also be simulated based on transient time-stepping FEA [2]. However, this method is very time consuming especially when multiple strands are used.

Iron loss produced in a magnetic material operating in an alternating magnetizing field is generally separated into two components: hysteresis loss and eddy current loss. Hysteresis loss is due to a form of intermolecular friction when a varying magnetic field is applied to the magnetic material. The loss per cycle is proportional to the area enclosed by the hysteresis loop on the B-H characteristics of the material. The hysteresis loss increases with the maximum magnetic field, as illustrated in Fig. 1.

The empirical formula expressing the hysteresis loss per unit volume (P_h (W/m^3)) in terms of the maximum flux density (B (T)) and frequency (f (Hz)) was developed by Steinmetz [3] as follows:

$$P_h = \eta B^n f \tag{7}$$

where η is a material constant and n is an exponent, which has typical values between 1.8 and 2.2, depending on the lamination material [4].

The term "eddy current" refers to circulating electric currents that are induced in a sheet of a conducting material when it is subjected to alternating magnetic field. These eddy currents produce power that is dissipated as heat. The eddy current loss per unit volume (P_e (W/m^3)), at frequencies which are low enough for the inductive effects to be neglected, is given by the following general equation [3]:

$$P_e = \frac{\pi^2 B^2 t^2 f^2}{\rho\beta} \tag{8}$$

where t is the thickness of the material (m), B is the peak flux density (T), ρ is the resistivity of the material (Ω m), and β is a coefficient that is related to the geometric structure.

Eddy current loss can also be divided into classical eddy current loss and excess eddy current loss for a more accurate analysis. Therefore, at a given frequency (f), the iron loss for electrical steel can be calculated from [5,6]

$$P_{\text{iron}} = k_h B^2 f + K_c (Bf)^2 + K_e (Bf)^{3/2} \tag{9}$$

where K_h, K_c, and K_e are the coefficients of hysteresis loss, classical eddy current loss, and excess eddy current loss, respectively, and B is the peak flux density. The coefficients can be calculated using the curve fitting of the iron loss data from manufacturers or from material test data.

The above equation is based on the assumption of sinusoidal excitation. When the iron core is subjected to the nonsinusoidal magnetic field, the distorted excitation, which can be represented by higher order harmonics, has to be considered [7,8]. The iron loss model considering arbitrary magnetic flux waveforms can be found in Ref. [9]. The transient time-stepping finite element method is also widely used to directly simulate the core loss [10,11].

Soft magnetic materials form the magnetic circuit in an electric machine. An ideal material would have high permeability in order to reduce the reluctance of the magnetic circuit, high saturation flux density in order to minimize the volume and weight of the iron core, and low losses. However, it is impossible to optimize all of these properties in a single material. This is because there are a large number of factors that affect magnetic properties (chemical composition, mechanical treatment, and thermal treatment are the most important), and the result is often a compromise. For example, nickel steel has low iron loss but low saturation flux density, while cobalt steel has higher saturation flux density but also higher iron loss. The iron core of a machine is made up of thin laminations in order to reduce core loss. Laminations as thin as 0.127 mm are generally used in high frequency applications in order to reduce iron loss.

Besides the laminated core, there are also two alternative materials [12]: (a) Amorphous metals (such as metglas), instead of their polycrystalline structure, have very low hysteresis and eddy current losses. Amorphous metals are produced by rapid cooling of alloys consisting of iron, nickel, and /or cobalt together with one or more of the following metalloids, which are elements or compounds exhibiting both metallic and nonmetallic properties: boron, silicon, and carbon. (b) Powder materials (such as grain-oriented electrical steels), in spite of their rather low core permeance, may be attractive for their very high frequency applications and also on account of their effective damping of vibrations.

2.2 Rotor Loss. The rotor loss generated by induced eddy current in the steel shaft and permanent magnets is not significant compared with the total machine loss. However, removing the heat from the rotor to ensure reasonable operating temperatures of its components is more difficult than removing the heat from the stator. Thus, an accurate prediction of rotor loss becomes important especially at high speed. The major causes of the rotor eddy current loss can be categorized into the following three groups: (a) no-load rotor eddy current loss caused by the existence of slots, (b) on-load rotor eddy current loss induced by the harmonics of windings' magnetomotive force (MMF), which is also called space harmonics, and (c) on-load rotor eddy current loss induced by the time harmonics of the phase currents due to PWM.

Loss due to eddy current, in general, can be expressed by

$$P = \int_V \sigma \mathbf{E}^2 dV = \int_V \mathbf{J}^2/\sigma dV \tag{10}$$

where σ is the material conductivity, $\mathbf{E}$ is the electric field, $\mathbf{J}$ is the eddy current density, and V is the volume of the material. For an accurate assessment, the rotor loss is generally simulated using a 2D FEA time-stepping transient solver with motion, in which the actual measured motor/generator current waveforms are applied. For alternators with a passive rectifier, the 2D FEA transient

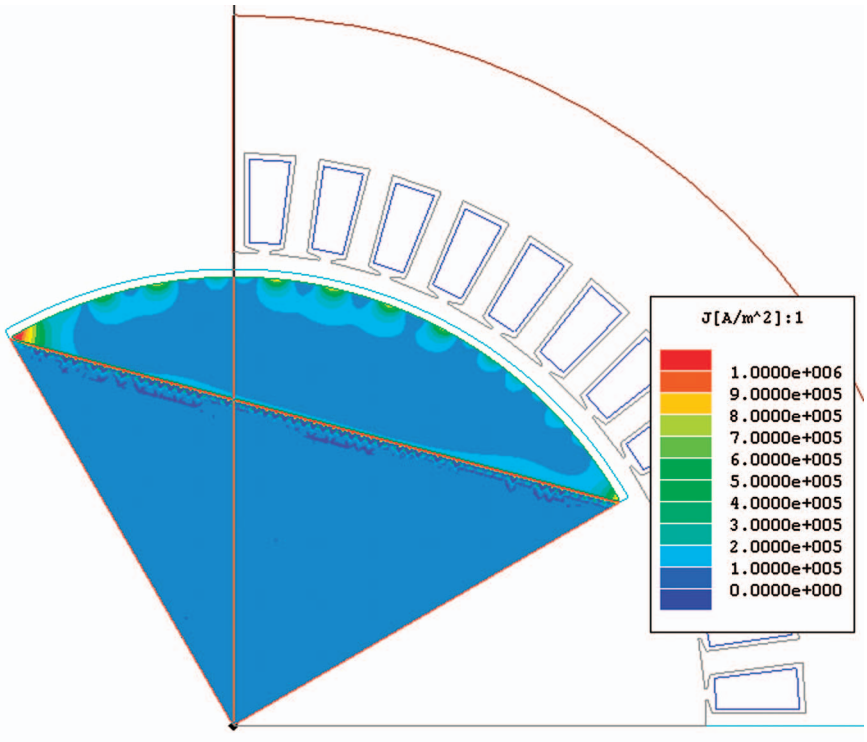

Fig. 2 Eddy currents in the rotor

solver with motion and external circuits can be used to simulate rotor loss and alternator performance. Figure 2 shows one example of eddy currents in the rotor caused by slot effect, winding space harmonics, and phase current time harmonics.

There are several methods to reduce rotor eddy current losses. Reducing the slot opening and increasing the magnetic gap between rotor and stator can reduce no-load rotor loss. Increasing the number of slots per pole and using fractional winding can reduce rotor loss caused by the space harmonics of the armature winding. Increasing the switching frequency and using external line inductors can reduce rotor loss caused by time harmonics of the phase currents. Since rotor loss caused by time harmonics is dominant in most applications, increasing the switching frequency and using external line inductance to reduce current THD is a very effective way to reduce rotor loss.

2.3 Windage Loss. Windage loss is heat generated in the fluid due to the relative motion (shearing) of the fluid that flows between the rotor and stator [13]. Windage loss, depending on various gases at various operating conditions, as used in high speed machines can be very high, contributing to overall machine inefficiency. The windage loss generation is a function of shaft rotational speed and fluid properties such as temperature, pressure, density, and temperature gradients at stator and rotor walls.

The windage loss generated in the clearance between a rotating cylinder and a stationary cylinder with homogenous laminar flow (no axial flow) can be estimated from the following system of equations [13].

Shaft rotational speed:

$$\omega = \frac{2\pi N}{60} \tag{11}$$

Reynolds number:

$$\mathrm{Re} = \omega r \frac{\rho}{\mu} \phi \tag{12}$$

Skin friction coefficient (C_d) for turbulent flow:

$$\frac{1}{\sqrt{C_d}} = 2.04 + 1.768 \ln(\mathrm{Re}\sqrt{C_d}) \tag{13}$$

Windage:

$$W = C_D \pi \rho \omega^3 r^4 \lambda \tag{14}$$

where N=rotational speed of rotor (in rpm), ρ=density of fluid (in kg/m^3), μ=kinematic viscosity of cooling media (in m^2/s), r=radius of the rotor (in m), φ=radial gap between rotor and stator (in m), and λ=length of the rotor (in m).

Theoretical relations and experimental validation taking into account the combination of axial flow and rotational flow, in the case of cooling media passing through the gap, can be included to obtain a better estimate. Also, surface roughness of the stator tooth and rotor surface affects windage loss and must be taken into account [14].

3 Typical Alternator Design and Loss Calculation

The detailed loss breakdown of a 120 kW alternator is provided as an example. The cross section of the alternator is shown in Fig. 3. Basic alternator performance parameters are shown in Table 1. The stator core is made of 0.178 mm silicon steel, and the length is 162 mm. The alternator output is connected to a passive rectifier shown in Fig. 4. A 2.86 Ω power resistor is used as an equivalent load to provide 120 kW output power.

The alternator performance was simulated using transient FEA with external circuit, and the result is summarized in Table 2. The phase current waveforms are also plotted in Fig. 5.

Based on Eq. (1), the copper I^2R loss is calculated to be 1167 W. According to Eq. (4), the resistance coefficient is 1.12, so the total copper loss is 1308 W (including 141 W of copper stray load loss). The air density at 77°C is 1.009 kg/m^3 and the viscosity is 2.075 m^2/s. According to Eqs. (11)–(14), the Reynolds number (Re) is equal to 14,179, the skin friction coefficient (C_d) is equal to 4.928×10^{-3}, and the windage loss is calculated to be 874 W.

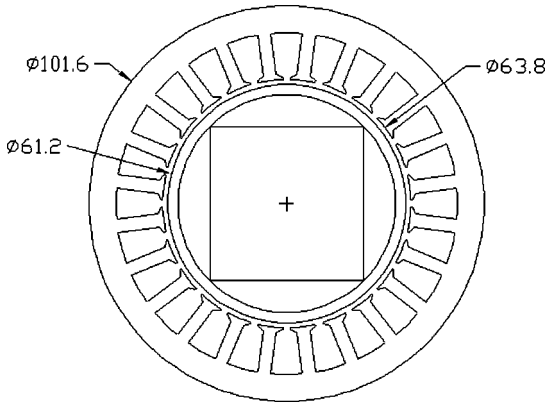

Fig. 3 The cross section of a 120 kW alternator (unit is in mm)

Based on the curve fitting of the manufacturer's data using a genetic algorithm, we get the coefficients of Eq. (9) as

$$K_h = 0.0275 \frac{W}{\text{Hz T}^2 \text{ kg}} \tag{15}$$

$$K_c = 1.83 \times 10^{-5} \frac{W}{\text{Hz}^2 \text{ T}^2 \text{ kg}} \tag{16}$$

$$K_e = 0.000277 \frac{W}{\text{Hz}^{1.5} \text{ T}^{1.5} \text{ kg}} \tag{17}$$

Table 1 Parameters of the motor/generator

Machine type	PM synchronous
Operating speed	70,000 rpm
Number of phases	3
Number of slots	24
Number of conductor /slot	6
Number of circuits	2
Winding resistance (line neutral)	16.3 mΩ @ 150°C (excluding leads)
Winding leakage inductance (per phase)	40 μH
D-axis magnetizing inductance (Lad)	39.3 μH
Q-axis magnetizing inductance (Laq)	54.6 μH
L-L Back EMF constant (V_{rms}/krpm)	8.26
Weight of core iron (kg)	2.37
Weight of teeth iron (kg)	1.20

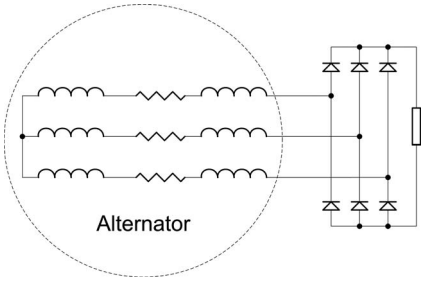

Fig. 4 Passive rectifier circuits

Table 2 Simulated performances

Output dc voltage (V)	583.7
Output dc current (A)	204.1
Output phase current (A_{rms})	154.5

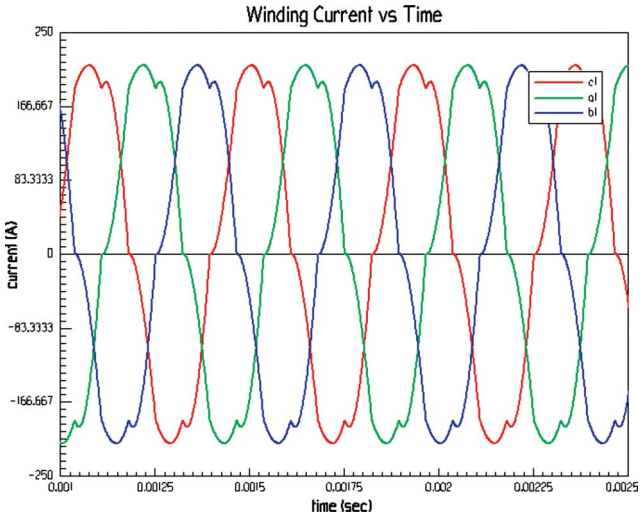

Fig. 5 Simulated current waveforms

According to FEA, the peak flux density is 1.45 T in the core and 1.17 T in the teeth. Therefore, according to Eq. (9), the core loss is calculated to be 945 W and teeth loss is computed to be 317 W. For rotor loss, the FEA simulation with a motor current waveform due to a passive rectifier was performed, and the rotor loss was found to be 221.9 W. The rotor loss due to current time harmonics is dominant because of high current harmonic distortions when using a passive rectifier. In summary, the losses of the high speed alternator at a rated load, excluding power electronics losses, are shown in Table 3.

4 Verification of Losses

Various methods can be used to verify alternator losses and operating efficiency.

4.1 Back-to-Back Test. For high speed machines, a back-to-back test configuration is most widely used to map machine performance at various load conditions from no load to full load. In this test, two identical machines are coupled together, with one operating as a motor and the other as a generator or load. Figure 6 shows a typical back-to-back test setup.

By measuring the input power to the motor and the output power from the generator, we can measure the total losses of the system that includes both units at various load conditions. Since the two machines are identical, we can calculate the total loss for each machine without introducing significant errors by compensating for small differences in winding losses due to the different operating current in each machine. For a more accurate assessment, a torque meter (if available) can also be used to directly measure the torque between the motor and generator.

Table 3 Summary of losses at a rated load

Stator loss	
Copper loss (W)	1308
Iron loss (W)	1262
Rotor loss	
Shaft loss (W)	15.9
PM loss (W)	206
Windage loss (W)	874
Total loss (W)	3666
Rated output power (W)	120,000
PM alternator efficiency (%)	97.0

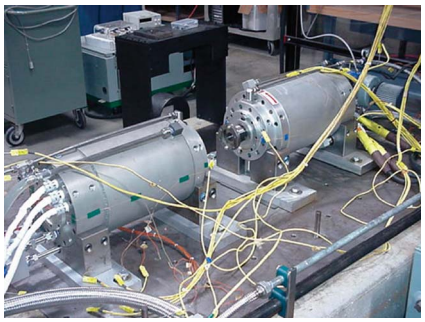

Fig. 6 Back-to-back test setup

4.2 Spin-Down Test. The relationship between the electromagnetic torque and the inertia torque is as follows:

$$T_{\text{em}} = J\frac{d\omega_r}{dt} + T_{\text{damp}} - T_{\text{mech}} \tag{18}$$

where T_{em} is the electromagnetic torque, T_{damp} is the damping torque in the direction opposite to rotation because of the friction, windage, and iron losses, T_{mech} is the externally applied mechanical torque in the direction of the rotor speed, and J is the rotor inertia.

A spin-down test is a method to measure the damping torque. When the motor is free spinning without externally applied mechanical torque and electromagnetic torque, Eq. (18) becomes

$$T_{\text{damp}} = -J\frac{d\omega_r}{dt} \tag{19}$$

Therefore, the motor losses can be calculated as

$$P_{\text{loss}} = -J \cdot \omega_r \frac{d\omega_r}{dt} \tag{20}$$

By measuring the initial speed versus time duration of the rotor from the initial speed to fully stop, the power loss can be calculated. When performing the spin-down test, any armature electrical loops should be disconnected to ensure that the motor is spinning down freely without any braking effect. If there is output power during the spin-down test, this power has to be considered in the calculation.

As an example, Fig. 7 shows the measured spin-down time versus rotor speed for a magnetic bearing supported high speed PM machine. The machine also produced output power of 140 W at 36,000 rpm, and 60 W at 8000 rpm during spin-down. The inertia of the entire rotating assembly is 0.68 kg m^2. Figure 8 shows the calculated total no-load loss versus rotor speed according to Eq. (20). The copper loss can be ignored in the calculation due to the very low output power.

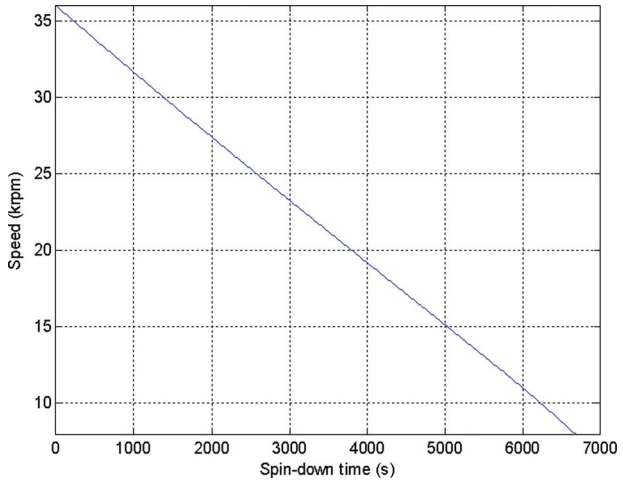

Fig. 7 Measured machine spin-down time versus rotor speed

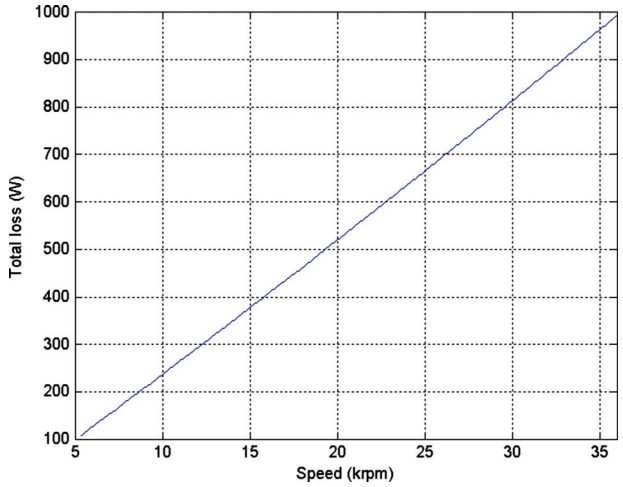

Fig. 8 Calculated no-load total loss versus speed

4.3 Temperature Mapping and Correlation With Thermal Model. In this technique, the machine is well instrumented throughout with temperature sensors such as thermocouples or thermistors. Temperature measurements are then made for various operating conditions with different loads and speeds. A finite difference thermal model of the machine is also constructed with calculated losses assigned for various components of the machine. Figure 9 shows a typical machine thermal model.

By adjusting losses in the thermal model so that predicted temperatures match the measured results for various operating conditions, we can estimate roughly different loss components of the machine. The validity of this technique depends significantly on the accuracy of the thermal model. Therefore this technique is often used as a secondary check.

5 Conclusion

High speed PM machines possess many desirable attributes that make them attractive for direct drive applications such as microturbines. In this paper, we describe the losses in high speed PM machines in detail. A typical PM machine designed for microturbine application is presented, and various verification methods are discussed. An accurate assessment of a machine's losses is critical in doing system design tradeoffs as well as in predicting system performance and ensuring a safe and reliable system operation.

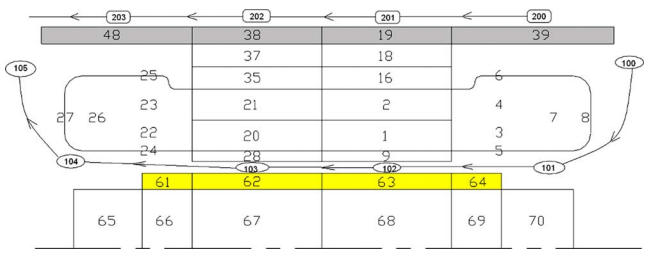

Fig. 9 A typical lumped parameter thermal model of a PM machine

References

[1] Lammeraner, J., and Stafl, M., 1966, *Eddy Currents*, CRC, Boca Raton, FL.

[2] Zheng, L., Wu, T. X., Acharya, D., Sundaram, K. B., Vaidya, J., Zhao, L., Zhou, L., Murty, K., Ham, C. H., Arakere, N., Kapat, J., and Chow, L., 2005, "Design of a Super-High Speed Permanent Magnet Synchronous Motor for Cryogenic Applications," *Proceedings of the IEEE International Electric Machines and Drives Conferences, IEMDC'05*, San Antonio, TX, May, pp. 874–881.

[3] Hamdi, E. S., 1994, *Design of Small Electrical Machines*, Wiley, New York.

[4] Mi, C., Slemon, G. R., and Bonert, R., 2003, "Modeling of Iron Losses of Permanent Magnet Synchronous Motors," IEEE Trans. Ind. Appl., **39**(3), pp. 734–742.

[5] Binesti, D., and Ducreux, J. P., 1996, "Core Losses and Efficiency of Electrical Motors Using New Magnetic Materials," IEEE Trans. Magn., **32**(5), pp. 4887–4889.

[6] Smith, A. C., and Edey, K., 1995, "Influence of Manufacturing Processes on Iron Losses," Proceedings of the IEE Electrical Machines and Drives Conference, Durham, UK, Sept., pp. 77–81.

[7] Slemon, G. R., and Liu, X., 1990, "Core Losses in Permanent Magnet Motors," IEEE Trans. Magn., **26**(5), pp. 1653–1655.

[8] Emanuel, E., 1988, "The Effect of Nonsinusoidal Excitation on Eddy Current Losses in Saturated Iron," IEEE Trans. Power Deliv., **3**(2), pp. 662–671.

[9] Roshen, W., 2007, "Iron Loss Model for Permanent Magnet Synchronous Motors," IEEE Trans. Magn., **43**(8), pp. 3428–3434.

[10] Chari, M. V. K., 1980, "Finite Element Analysis of Electrical Machinery and Devices," IEEE Trans. Magn., **16**(5), pp. 1014–1019.

[11] Shimoji, H., 2001, "Iron Loss and Magnetic Fields Analysis of Permanent Magnet Motors by Improved Finite Element Method With E&S: Model," IEEE Trans. Magn., **37**(5), pp. 3526–3529.

[12] de Jong, H. C. J., 1989, *AC Motor Design: Rotating Magnetic Fields in a Changing Environment*, Hemisphere, Chap. 2, pp. 14–15.

[13] Vrancrik, J. E., 1968, "Prediction of Windage Power Loss in Alternators," NASA-Langey, Report No. TND-4849.

[14] Becker, K. M., and Kaye, J., 1962, "Measurement of Diabetic Flowin Annulus With an Inner Rotating Cylinder," ASME J. Heat Transfer, **84**, pp. 97–105.